Science and Technology Indonesia
e-ISSN:2580-4391 p-ISSN:2580-4405
Vol. 11, No. 2, April 2026

Research Paper

Anticancer Activity of Trisubstituted Pyrazoline Derivatives: Synthesis, Characterisation, and Computational Studies

Sabah Motrud Mazal[1], Zainab Al-Shuhaib[1*], Raed Awad Alharis[1], Kawkab Ali Hussein[1], Sadiq Muhammad Hassan Ismail[1]

[1]*Department of Chemistry, College of Education for Pure Sciences, University of Basrah, Basrah, 61004, Iraq*
*__Corresponding author__: zainab.saleh@uobasrah.edu.iq

Abstract
The search for new anticancer drugs that target apoptotic and autoimmune pathways is essential, as these pathways are crucial for maintaining cellular homeostasis and destroying cancer cells. In this study, eight trisubstituted pyrazoline derivatives (2a-2d and 3e-3h) were made by mixing chalcones with hydrazide derivatives (hydrazine hydrate and phenyl hydrazide) in a cyclocondensation process. The EI-MS, ^{1}H NMR, ^{13}C NMR, and ^{19}F NMR spectra were utilized to describe these variants. The MTT test was utilized to see how harmful they were to the MCF-7 tumor cell type. The results exhibited that compounds 2a-2d demonstrated the strongest inhibitory impact on MCF-7 proliferation, with IC_{50} values of 19.46, 29.45, 44.15, and 26.37 μg/mL after 24 hours of exposure. Among them, compound 2a was the most potent. By comparison, compounds 3e-3h had significantly higher IC_{50} values of 101.67, 75.99, 102.83, and 99.54 μg/mL than the reference medication doxorubicin, which has an IC_{50} of 1.24 μg/mL. Additionally, docking of compound 2a exhibited strong binding affinity values with the protein (PDB ID: 5T92) amino acid residues across several interactions, including hydrogen acceptor, hydrogen donor, and hydrogen-pi, as well as two hydrogen acceptor and pi-hydrogen contacts with the other amino acids and water. The most favourable binding pose corresponded to the lowest ΔG and exhibited robust pose quality. Based on the 6-311+G(d) basis set and the B3LYP functional, the molecular structures of compounds 2a–d have been optimized, and molecular orbital studies utilized to examine their quantum chemical characteristics.

Keywords
Anticancer, Chalcones, Cyclocondensation, DFT, Molecular Docking, Pyrazoline

Received: 13 December 2025, Accepted: 4 March 2026
https://doi.org/10.26554/sti.2026.11.2.661-676

1. INTRODUCTION

Pyrazolines are a serious type of heterocyclic compounds that have enchanted substantial consideration in chemical pharmacy simply because of their many therapeutic uses (Abou-Zied et al., 2024). Among these, the therapeutic value of pyrazoline-based scaffolds has been widely explored, owing to their favourable structural flexibility and their ability to cooperate with multiple biochemical substances (Khan et al., 2026; Nehra et al., 2025). Structural modification through appropriate substitution has been shown to significantly influence their pharmacological behaviour, making pyrazoline derivatives promising candidates for further drug development (Dadang, 2025; Reddy et al., 2025).

Prior works have shown that cytotoxic action is significantly altered by the kind and location of substituents on the pyrazoline ring (Hassan et al., 2024; Manwar et al., 2025; Yadav et al., 2024). However, much of the reported literature has focused on mono- or disubstituted pyrazoline frameworks or has emphasised biological screening without detailed mechanistic interpretation at the molecular level (Reddy et al., 2024).

Additionally, in an effort to use more environmentally friendly chemistry techniques. Pyrazolines have been synthesized from benzylideneacetophenone using costly catalysts. The problem of orientation in the pyrazoline preparation process, however, is a common obstacle to all of these approaches (Nair et al., 2025; Khan et al., 2024). The lack of orientation represents a major challenge. Mechanistically, these reactions usually result in the formation of both homologous compounds, which pose problems for product yield and require complex separation methods. Accordingly, there has been a continuous interest in developing simple, effective, and eco-friendly methods for the synthesis of pyrazolines because of their high bioavailability and wide range of uses in chemical synthesis (Abbas et al., 2024; Hameed et al., 2025).

In view of the above, the present study was undertaken to bridge the gap by rationally designing two new series of structurally diverse trisubstituted pyrazoline derivatives through the cyclocondensation of chalcones with hydrazine hydrate

and phenyl hydrazine under optimized reflux conditions. The newly synthesized compounds were characterized extensively, and their in vitro cytotoxicity was screened against the human breast cancer cell line MCF-7 utilizing a colourimetric assay. To elucidate the mechanism underlying the observed bioactivity, the potent compounds were subjected to molecular docking studies against the oestradiol-binding domain of oestradiol receptor α (PDB ID: 5T92). Furthermore, the study was extended to calculate frontier molecular orbitals, energy gaps, chemical reactivity descriptors, and statistical correlations with anticancer activity, utilizing density functional theory (DFT) at the B3LYP/6-311+G(d) level, along with in silico ADMET predictions to assess the compounds' pharmacokinetic suitability. b

2. EXPERIMENTAL SECTION

2.1 Materials

Materials utilised included 4-Bromoacetophenone (98%, Merck), 4-Fluorobenzaldehyde (98%, Merck), 4-Nitroacetophenone (98%, Merck), 4-(Methylthio)benzaldehyde (97%, Sigma-Aldric h), 4-Fluoroacetophenone (98%, Merck), 3,4-dimethylacetophe none (97%, Sigma-Aldrich), 4-(Trifluoromethyl)benzaldehyde (99%, Sigma-Aldrich), and p-Formylnitrobenzene (98%, Sigma -Aldrich).

2.2 Instrument

A Thermoscientific melting point device, a Bruker ARX-400 NMR spectrometer, and an MS model 5975c VL MSD EI 70eV were utilized in this work.

2.3 Methods

2.3.1 Comprehensive Procedure for the Synthesis of Trisubstituted Pyrazoline Compounds 2a-2d

A condensation process was utilized to make the pyrazolines. A combination of chalcones 1a-1d (10 mmol) and 40 mmol of 80% hydrazine monohydrate in 20 mL of methanecarboxylic acid was preheated to 90°C in a flask with a round bottom. Following 72 hours of heating, the solution was chilled to normal temperature and then put in a bath of ice to cause the solid to precipitate. It was neutralised with 1-hydroxyethane and water, dried and recrystallised from 1-hydroxyethane to purify it.

2.3.1.1 1-(3-(4-Bromophenyl)-5-(4-Fluorophenyl)-4,5-Dih ydro-1H-Pyrazol-1-yl)Ethan-1-One (2a)

The yield is 68%, R_f = 0.43 (EtAc/Hex, 4/6 v/v). It has a m.p. of 164–166 °C and is white, crystalline. The ^{1}H NMR spectrum (DMSO), Δ_H (ppm): 2.30 (s, 3H, $COCH_3$ group), 3.11 (dd, CH_2 pyrazole ring, J = 18.1, 4.8 Hz, 1H), 3.83 (dd, CH_2 pyrazole ring, J = 18.2, 11.9 Hz, 1H), 5.55 (dd, CH pyrazole ring, J = 11.9, 4.7 Hz, 1H), 7.14 (t, 2H), 7.23 (t, 2H), 7.65 (d, 2H), 7.71 (d, 2H). The ^{13}C NMR spectrum (DMSO), Δ_C (ppm): C21 (22.2), C12 (42.3), C11 (59.5), aromatic carbons (115.7–138.8), C7 (138.9), C16 (153.7 and 163.0), C20 (168.0). The ^{19}F NMR spectrum, Δ_F (ppm): -115.4 (s, 1F). MS [EI]$^+$: m/z = 360.1 [M]$^+$.

2.3.1.2 1-(3-(4-Bromophenyl)-5-(4-(Methylthio)Phenyl)-4,5-Dihydro-1H-Pyrazol-1-yl)Ethan-1-One (2b)

The yield is 62%, R_f = 0.51 (EtAc/ Hex, 4/6 v/v). It has a m.p. of 176–178 °C, a yellow crystalline. The ^{1}H NMR spectrum in DMSO, Δ_H (ppm): 2.30 (s, 3H, $COCH_3$ group), 2.44 (s, 3H, SCH_3 group), 3.12 (dd, CH_2 pyrazole ring, J = 18.1, 4.4 Hz, 1H), 3.83 (dd, CH_2 pyrazole ring, J = 18.1, 11.9 Hz, 1H), 5.51 (dd, CH pyrazole ring, J = 11.9, 4.7 Hz, 1H), 7.13 (d, 2H), 7.22 (d, 2H), 7.66–7.73 (m, 4H). In the DMSO ^{13}C NMR spectrum Δ_C (ppm): C23 (15.2), C20 (22.2), C12 (42.3), C11 (59.7), aromatic carbons (124.2–139.5), C7 (153.8), C19 (167.9). MS [EI]$^+$ m/z 388.2 [M]$^+$.

2.3.1.3 1-(5-(4-(Methylthio)Phenyl)-3-(4-Nitrophenyl)-4,5-Dihydro-1H-Pyrazol-1-yl)Ethan-1-One (2c)

The yield is 65%, R_f = 0.40 (EtAc/ Hex, 4/6 v/v). It has a m.p. of 167–169 °C, a yellow crystalline. In the DMSO ^{1}H NMR spectrum Δ_H (ppm): 2.33 (s, 3H, $COCH_3$ group), 2.44 (s, 3H, SCH_3 group), 3.21 (dd, CH_2 pyrazole ring, J = 18.2, 4.9 Hz, 1H), 3.90 (dd, CH_2 pyrazole ring, J = 18.2, 12.0 Hz, 1H), 5.56 (dd, CH pyrazole ring, J = 12.2, 4.9 Hz, 1H), 7.14–7.23 (m, 4H), 8.02 (d, 2H), 8.30 (d, 2H). The ^{13}C NMR spectrum in DMSO, Δ_C (ppm): C25 (15.2), C19 (22.2), C11 (42.2), C10 (60.2), aromatic carbons (124.4–139.2), C5 (148.4), C7 (152.9), C18 (168.3). MS [EI]$^+$ m/z 355.1 [M]$^+$.

2.3.1.4 1-(3-(4-Fluorophenyl)-5-(4-(Methylthio)phenyl)-4,5-Dihydro-1H-Pyrazol-1-yl)Ethan-1-One (2d)

The yield is 60%, R_f = 0.53 (EtAc/ Hex, 4/6 v/v). It has a m.p. of 150–152 °C, a white crystalline. The ^{1}H NMR spectrum in DMSO, Δ_H (ppm): 2.30 (s, 3H, $COCH_3$ group), 2.44 (s, 3H, SCH_3 group), 3.14 (dd, CH_2 pyrazole ring, J = 18.1, 4.2 Hz, 1H), 3.83 (dd, CH_2 pyrazole ring, J = 18.1, 11.8 Hz, 1H), 5.51 (dd, CH pyrazole ring, J = 11.8, 4.5 Hz, 1H), 7.13 (d, 2H), 7.22 (d, 2H), 7.31 (t, 2H), 7.84 (t, 2H). In the DMSO ^{13}C-NMR spectrum Δ_C (ppm): C23 (15.3), C20 (22.2), C12 (42.5), C11 (59.6), aromatic carbons (116.2–137.4), C7 (139.5), C6 (153.8 and 165.0), C19 (167.8). Fluori ne-19 NMR spectrum, Δ_F (ppm): -110.1 (s, 1F). MS [EI]$^+$ m/z: 328.1 [M]$^+$.

2.3.2 Overall Approach to Produce Trisubstituted Pyrazoline Derivatives 3e-3h

Chalcones 1e-1h (1 mmol) in absolute ethanol (20 mL) were combined with 1.5 mmol of phenyl hydrazine, treated with three drops of HCl, and refluxed at 90°C for 24 hours. Afterwards, the mixture was chilled to normal temperature, diluted with ice-cold water, and then kept overnight. Filtering was utilized to remove the precipitate, which was then neutralized by 1-hydroxyethane and water, dried, and purified by recrystallization from 1-hydroxyethane.

2.3.2.1 3-(3,4-Dimethylphenyl)-1-Phenyl-5-(4-(Trifluorom ethyl)Phenyl)-4,5-Dihydro-1H-Pyrazole (3e)

The yield is 74%, R_f = 0.4 (EtAc/ Hex, 4/6 v/v). It has a m.p. of 161–163 °C, a white crystalline. The ^{1}H NMR spectrum in DMSO, Δ_H (ppm): 2.25 (s, 3H, CH_3), 2.26 (s, 3H, CH_3), 3.10–3.18 (m, 1H, pyrazole ring), 3.92 (dd, CH_2 pyrazole ring, J = 17.5, 12.2 Hz, 1H), 5.60 (dd, CH pyrazole ring, J = 12.2, 6.0 Hz, 1H), 6.72 (t, 1H), 6.99 (d, 2H), 7.15–7.20 (m, 3H), 7.45–7.51 (m, 3H), 7.56 (s, 1H), 7.72 (d, 2H). In the DMSO ^{13}C NMR spectrum Δ_C (ppm): C13,25 (19.8), C3 (43.3), C1 (62.8), aromatic carbons (113.3–147.7), C4 (148.1). Fluorine-19 NMR spectrum, Δ_F (ppm): -60.9 (s, 3F, CF_3). MS [EI]$^+$ m/z: 394.3 [M]$^+$.

2.3.2.2 3-(4-Fluorophenyl)-5-(4-Nitrophenyl)-1-Phenyl-4,5-Dihydro-1H-Pyrazole (3f)

The yield is 72%, R_f = 0.51 (EtAc/ Hex, 4/6 v/v). It has a m.p. of 177–179 °C, a yellow crystalline. In the DMSO ^{1}H NMR spectrum Δ_H (ppm): 3.19 (dd, CH_2 pyrazole ring, J = 17.6, 6.3 Hz, 1H), 3.97 (dd, CH_2 pyrazole ring, J = 17.6, 12.4 Hz, 1H), 5.69 (dd, CH pyrazole ring, J = 12.4, 6.3 Hz, 1H), 6.75 (t, 1H), 6.99 (d, 2H), 7.17 (t, 2H), 7.28 (t, 2H), 7.57 (d, 2H), 7.80 (t, 2H), 8.22 (d, 2H). The ^{13}C NMR spectrum in DMSO, Δ_C (ppm): C3 (43.1), C1 (63.0), aromatic carbons (113.4–147.1), C22 (147.3), C4 (150.5), C10 (161.7 and 164.2). Fluorine-19 NMR spectrum, Δ_F (ppm): -112.1 (s, 1F). MS [EI]$^+$ m/z: 361.2 [M]$^+$.

2.3.2.3 3-(3,4-Dimethylphenyl)-5-(4-Nitrophenyl)-1-Phenyl-4,5-Dihydro-1H-Pyrazole (3g)

The yield is 76%, R_f = 0.6 (EtAc/ Hex, 4/6 v/v). It has a m.p. of 179–181°C, a yellow crystalline. The ^{1}H NMR spectrum in DMSO, Δ_H (ppm): 2.24 (s, 3H, CH_3), 2.26 (s, 3H, CH_3), 3.13 (dd, CH_2 pyrazole ring, J = 17.5, 6.1 Hz, 1H), 3.93 (dd, CH_2 pyrazole ring, J = 17.5, 12.3 Hz, 1H), 5.64 (dd, CH pyrazole ring, J = 12.3, 6.1 Hz, 1H), 6.73 (t, 1H), 6.99 (d, 2H), 7.17 (t, 3H), 7.45 (d, 1H), 7.55 (d, 3H), 8.21 (d, 2H). In the DMSO ^{13}C NMR spectrum, Δ_C (ppm): C9,10 (19.8), C3 (43.2), C1 (62.7), aromatic carbons (113.3–147.3), C23 (148.1), C4 (150.6). MS [EI]$^+$ m/z: 371.2 [M]$^+$.

2.3.2.4 3-(4-Fluorophenyl)-1-Phenyl-5-(4-(Trifluoromethyl)phenyl)-4,5-Dihydro-1H-Pyrazole (3h)

The yield is 71%, R_f = 0.53 (EtAc/ Hex, 4/6 v/v). It has a m.p. of 145–147 °C, a yellow crystalline. In the DMSO ^{1}H NMR spectrum Δ_H (ppm): 3.17 (dd, CH_2 pyrazole ring, J = 17.6, 6.2 Hz, 1H), 3.94 (dd, CH_2 pyrazole ring, J = 17.6, 12.3 Hz, 1H), 5.62 (dd, CH pyrazole ring, J = 12.3, 6.2 Hz, 1H), 6.74 (t, 1H), 7.00 (d, 2H), 7.17 (t, 2H), 7.27 (t, 2H), 7.51 (d, 2H), 7.71 (d, 2H), 7.79 (t, 2H). The ^{13}C-NMR spectrum in DMSO, Δ_C (ppm): C3 (43.2), C1 (63.2), aromatic carbons (113.4–147.0), C4 (147.5), C10 (161.7 and 164.1). Fluorine-19 NMR spectrum, Δ_F (ppm): -61.0 (s, 3F, CF_3), -112.2 (s, 1F). MS [EI]$^+$ m/z: 384.3 [M]$^+$.

2.4 Anticancer Activity

2.4.1 In Vitro Cytotoxicity of Synthesized Compounds Over Michigan Cancer Foundation-7

Growth and cultured line. Michigan Cancer Foundation-7 was handed by the National Cell Bank in Iran to the Institute of Pasteur. In RPMI-1640 medium (Gibco), the cells were cultured in the presence of 10% fetal bovine serum (Grand Island Biological Company [Gibco]) and streptomycin (100 μg/mL) and penicillin (100 μ/mL). Trypsin-ethylenediaminetetraacetic acid (EDTA) (Grand Island Biological Company [Gibco]) and PBS (phosphate-buffered saline) were used to flow cells through a humidified atmosphere at 37°C with 5% carbon dioxide. Growth was assessed in 3D clusters under the same circumstances and with the same fluids as cells grown on a single layer.

The thiazolyl blue tetrazolium bromide (MTT) experiment is utilized to see how alive cells are in the Michigan Cancer Foundation-7 (Nair et al., 2022; Becer et al., 2023). Cell proliferation and viability were assessed utilizing the thiazolyl blue tetrazolium bromide (MTT) experiment. A final density of 1.5×10^4 cells per well was achieved by trypsinizing, collecting, and adjusting the cells. After that, they were arranged in 96-well plates, each containing 200 μL of fresh medium, and the plates were left to warm for a whole day. Over 24 hours at 37°C in 5% carbon dioxide, compounds 2a-2d and 3e-3h were evaluated at concentrations that varied between 6.25 and 100 μg/mL and 12.5–200 μg/mL, respectively. At the last stage of the treatment period (24 hours), 200 μL/well of the thiazolyl blue tetrazolium bromide (MTT) solution (0.5 mg/mL in phosphate-buffered saline, or PBS) was included while the monolayer culture remained intact in the initial plate. Thus, the plate was incubated for an additional four hours at 37°C. After removing the thiazolyl blue tetrazolium bromide (MTT) solution, each well received 100 μL of dimethyl sulfoxide. At 37°C, cells were shaken until the crystals were completely dispersed. A microplate reader (Wave XS2, BioTek, USA) was utilized to calculate cell survival by recording absorbency at 570 nm. Dose-response curves were utilized to compute the IC_{50}, or the dosage of the chemicals that causes 50% dead cells. The reference standard was doxorubicin.

2.4.2 Statistical Analysis

The range values are presented to demonstrate experimental consistency, and the data are presented as mean ± SEM (n = 3) from independent experiments. Based on an analysis of variance (ANOVA) performed in GraphPad Prism 7 (2016), statistical significance was established as p <0.0001.

2.5 Ligand–Protein Molecular Docking

All docking and scoring algorithms were completed using the drug discovery software (Chemical Computing Group ULC, 2025). It is made up of the estrogen receptor alpha ligand binding region and (2E). The crystal structure of -3-4-[(1R)-2-(4-fluorophenyl)-6-hydroxy-1-methyl-1,2,3,4-tetrahydroiso- quinolin-1-yl] phenyl prop-2-enoic acid (PDB ID: 5T92) shows

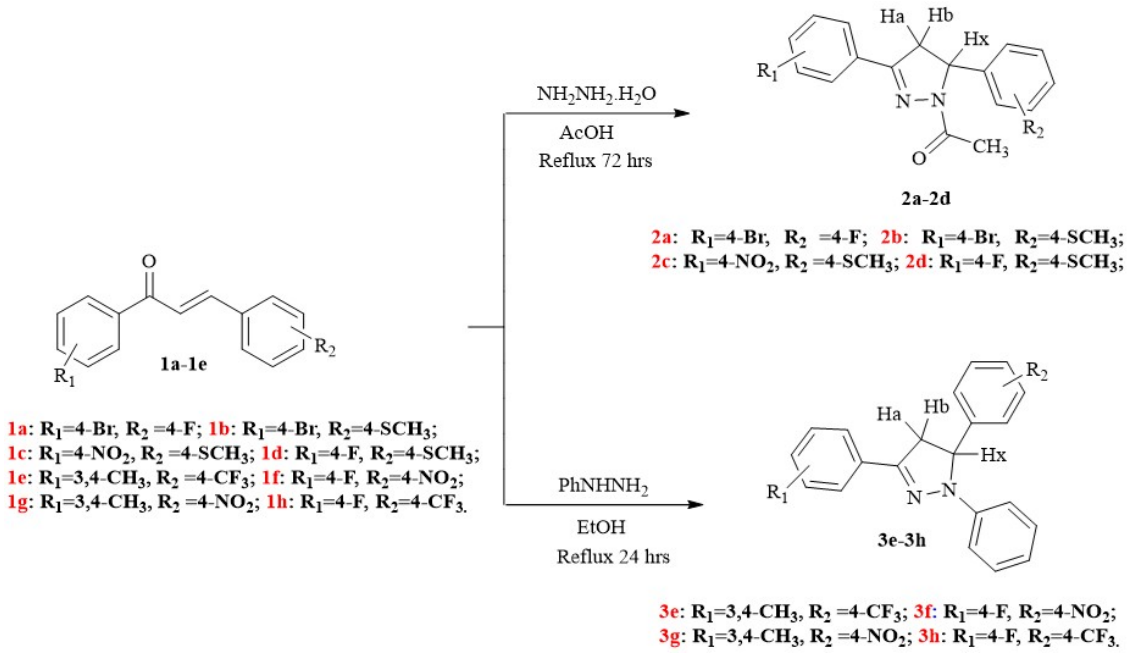

Figure 1. Synthetic Route of Pyrazolines 2a-2d and 3e-3h

Table 1. Cytotoxic Activity of the Evaluated Pyrazolines 2a–2d and 3e–3h in Combination with the DOX Drug Against the MCF-7 Cell Line

Comp. no.	Cell viability% (100 μg/mL)	IC_{50} (μg/mL)	Comp. no.	Cell viability% (200 μg/mL)	IC_{50} (μg/mL)
2a	15.02	19.46	3e	30.44	101.67
2b	22.85	29.45	3f	19.64	75.99
2c	32.02	44.15	3g	38.29	102.83
2d	13.89	26.37	3h	37.54	99.54
DOX	6.77	1.24	DOX	5.35	2.43

Table 2. Comparison of Anticancer Activity of Pyrazolone and Chalcone Derivatives Reported in the Literature with the Present Study

Comp. class	Key Structural Features	Cell Line IC_{50}	Reference
Pyrazolone derivative	Mono-/disubstituted pyrazolone scaffold	MCF-7 180–350 μg/mL	(Dimitris, 2020)
Pyrazolone derivative	Chalcone-derived pyrazolone	MCF-7 150–300 μg/mL	(Alsimaree, 2025)
Chalcone derivative	α, β-Unsaturated carbonyl system	MCF-7 222–818 μg/mL	(Patil et al., 2024)
This work	Trisubstituted pyrazolone derivatives	MCF-7 19.46–102.83 μg/mL	Present study

its shape. The data came from the Protein Data Bank and had a resolution of 2.22 Å. It is thought that docking studies are good enough when the precision is between 1.5 and 2.5 Å. Most people agree that the best RMSD (Root-Mean-Square Deviation) number is somewhere around 2 Å, and the energy score should be -7 kcal/mol or less. Both of these numbers are commonly utilized to be standards to ensure molecular docking data.

2.6 Details of the Computation

All of the calculations in this study, which utilized DFT (Density Functional Theory), were done with the Gaussian 16 software (Ali et al., 2024). The basis set 6-31G +(d) and hybrid functional (B3LYP) were utilized to figure out the features of the title molecules in this work (Frisch, 2016). Vibrational modes were also investigated to guarantee that no imaginary modes were present. The Gauss sum program is implemented to ana-

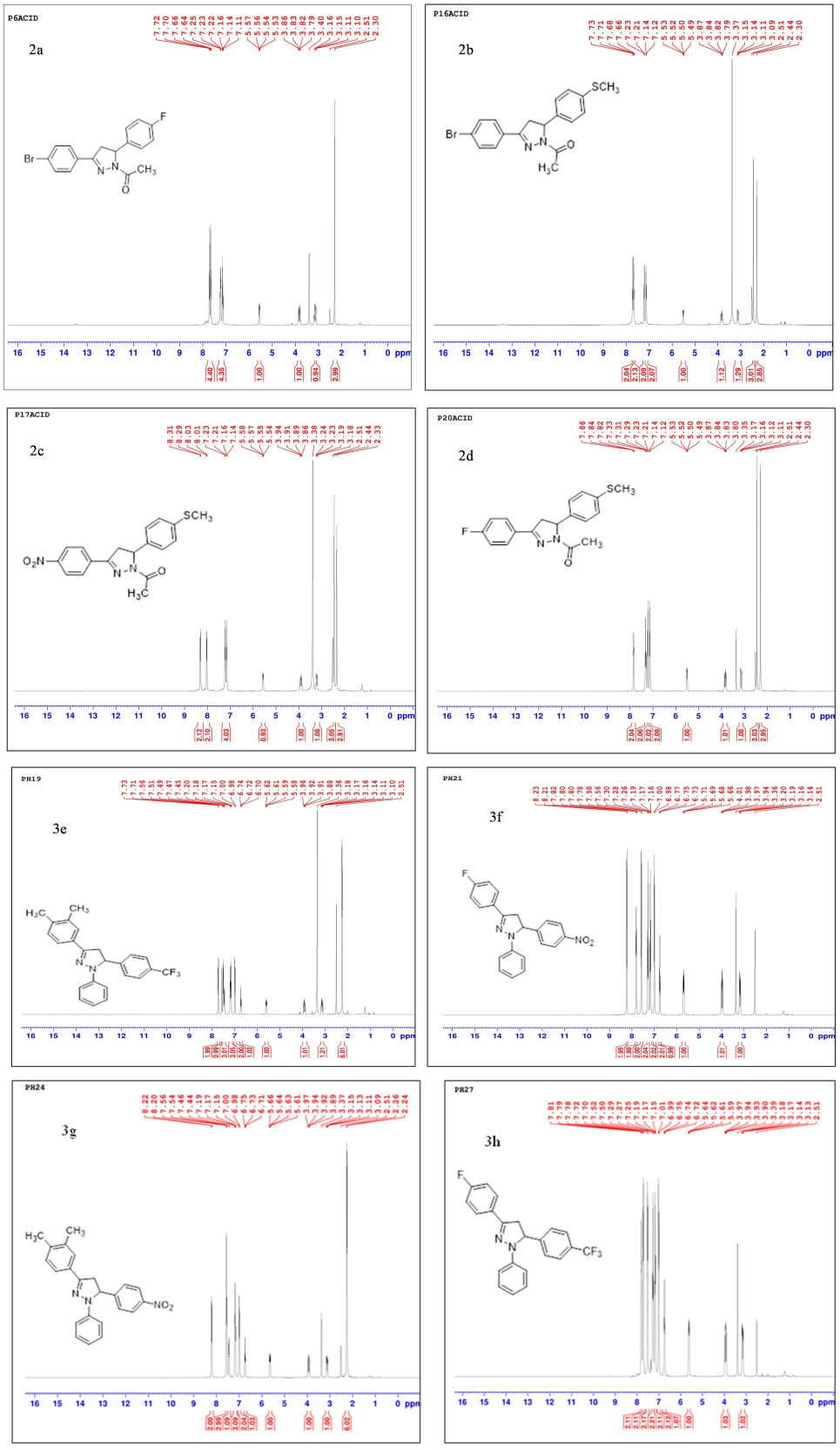

Figure 2. ^{1}HNMR Spectra of the Synthesized Compounds (2a-2d) and (3e-3h)

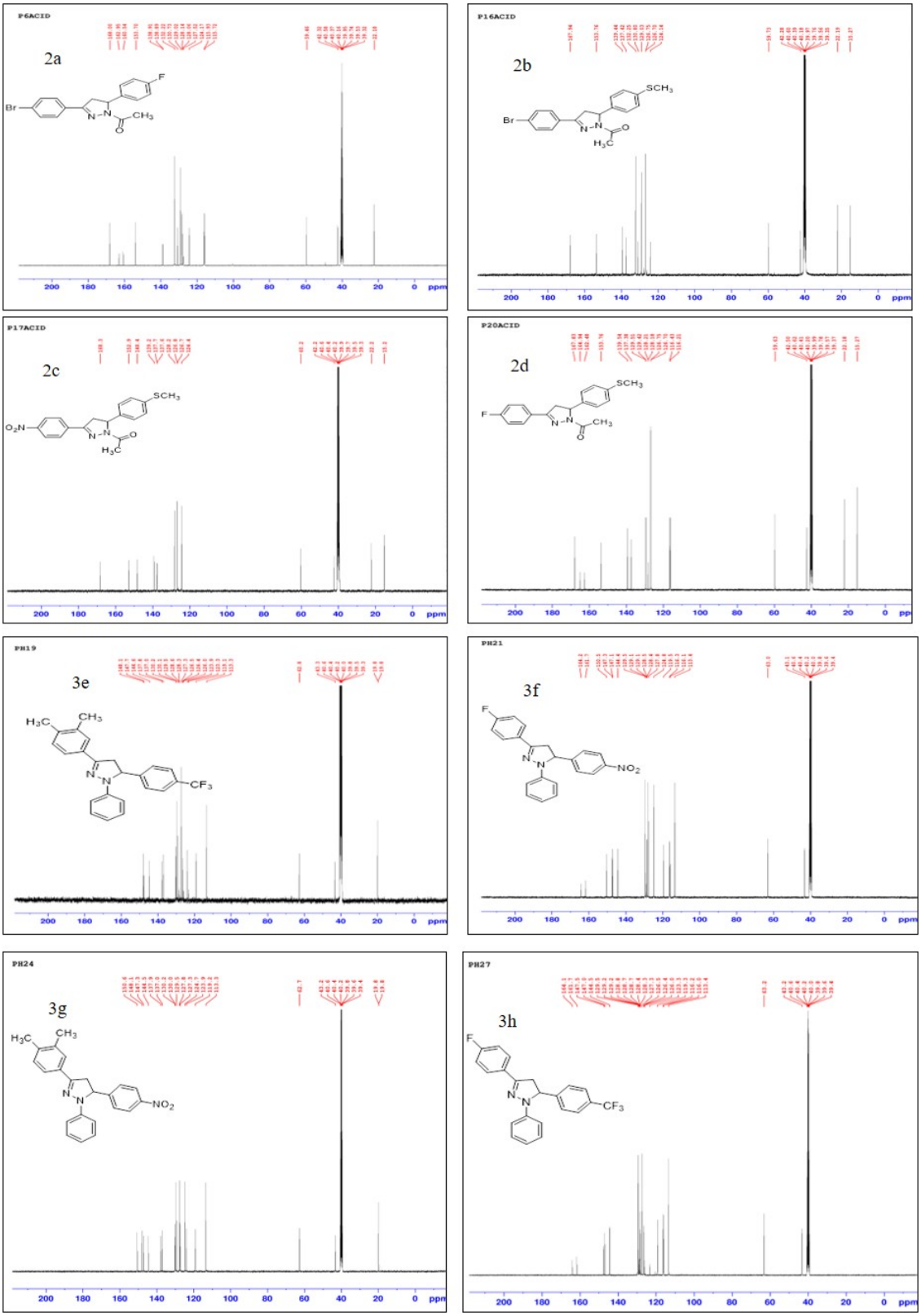

Figure 3. ^{13}CNMR Spectra of the Synthesized Compounds (2a-2d) and (3e-3h)

lyze DOS (Density of States) spectra (Baskerville et al., 2022; Zhang et al., 2020; Elkanzi et al., 2022).

3. RESULTS AND DISCUSSION

3.1 Chemistry

Claisen–Schmidt reaction of acetophenone with substituted aryl aldehydes was used to prepare the major intermediate benzylideneacetophenone under basic conditions (El-Sayed et al., 2022). As shown in Figure 1, the pyrazoline derivatives 2a-2d were formed by reacting the benzylideneacetophenones with hydrazine monohydrate in methanecarboxylic acid. Similarly, the benzylideneacetophenones were reacted with phenyl hydrazine, and a few drops of HCl were added to yield the pyrazoline derivatives 3e-3h. Structural validation was performed using ^{1}H, ^{13}C, ^{19}F NMR, and mass spectrometry (Ali et al., 2020).

The proton NMR spectra of the made compounds 2a–2d exhibited coupling between protons H_a and H_b at C12 and H_x at C11. H_a, presents as doublets of doublets at Δ 3.11–3.21 ppm (J_{ab} = 18.1–18.2 Hz and J_{ax} = 4.2–4.9 Hz). Around Δ 3.83–3.90 ppm, H_b occurs as a doublet of doublets (J_{ab} = 18.1–18.2 Hz and J_{bx} = 11.8–12.0 Hz). H_x occurs as a doublet of doublets around Δ 5.51–5.56 ppm (J_{bx} = 11.8–12.0 Hz and J_{ax} = 4.5–4.9 Hz). In the same context, the ^{1}H NMR of compounds 3e–3h exhibited coupling between H_a and H_b at C3 and proton H_x at C1. H_a occurs as a doublet of doublets at Δ 3.10–3.19 ppm (J_{ab} = 17.5–17.6 Hz and J_{ax} = 6.1–6.3 Hz). H_b presents as a doublet of doublets around Δ 3.92–3.97 ppm (J_{ab} = 17.5–17.6 Hz and J_{bx} = 12.2–12.4 Hz). H_x occurs as a doublet of doublets around Δ 5.60–5.69 ppm (J_{bx} = 12.2–12.4 Hz and J_{ax} = 6.0–6.3 Hz), as shown in Figure 2.

The structures of the generated compounds were verified by the following indicators in the ^{13}C NMR spectra of compounds 2a–2d: signals between Δ 42.2–42.5 ppm are assigned to the CH_2 group, while those between 59.5 and 60.2 ppm are assigned to the CH group of the pyrazoline ring. The signals between 115.7 and 139.5 ppm correspond to aromatic carbons, those between 138.9 and 153.8 ppm to the C=N group, and those between 167.8 and 168.3 ppm to the C=O group. The same applies to compounds 3e–3h; the spectra show signals between Δ 43.1 and 43.3 ppm corresponding to the CH_2 group; signals between 62.7 and 63.2 ppm related to the CH group of the pyrazoline ring; and signals between 147.5 and150.6 ppm corresponding to the C=N group, as shown in Figure 3.

Furthermore, the ^{19}F NMR spectra of compounds 2a and 2d exhibited singlet signals at -115.4 and -110.1 ppm, indicating the presence of the F substituent. The same applies to compounds 3e, 3f, and 3h, which exhibited singlet signals at -60.9, -112.1, -61.0, and -112.2 ppm, corresponding to the CF_3 and F substituents (Figure 4).

Additionally, the MS $[EI]^+$ analysis of pyrazolines 2a–2d peaks of molecular ion occur at m/z 360.1, 388.2, 355.1, and 328.1, respectively, closely matching the predictable values of m/z 360.03, 388.02, 355.10, and 328.10. So it is with molecules 3e–3h, which have molecular ion peaks at m/z 394.3 (M^+), 361.2 (M^+), 371.2 (M^+), and 384.3 (M^+), in that order. The estimated m/z values of 394.17, 361.12, 371.16, and 384.12 are very close to the peaks that were seen (Figure 5).

3.2 Anti-Cancer Assay in Vitro

The anticancer activity of the pre-processed compounds 2a-2d, tested between 6.25 and 100 μg/mL, and compounds 3e-3h, tested from 12.5-200 μg/mL, was evaluated versus the human breast cancer cell line MCF-7 utilized a cell viability assay. As shown in Table 1 and Figure 6, compounds 2a-2d displayed a dose-dependent decrease in cell viability, with higher concentrations causing a steady decline in viable cells. At the highest tested concentration of 100 μg/mL, cell viability dropped to 15.02%, 22.85%, 32.02%, and 13.89%, respectively, compared to the untreated control. The dose-response data analysis revealed IC_{50} values of 19.46, 29.45, 44.15, and 26.37 μg/mL. These values indicate the concentrations required to inhibit 50% of MCF-7 cell viability, with compound 2d showing the lowest cell viability (13.89%) and the most potent cytotoxicity at 100 μg/mL. However, compound 2a has the lowest IC_{50} value (19.46 μg/mL), meaning it requires the lowest concentration to inhibit half of the cells. Similarly, compounds 3e-3h revealed a dose-dependent reduction in cell viability, with higher concentrations resulting in a gradual decrease in viable cells. At the highest tested concentration of 200 μg/mL, cell viability decreased to 30.44%, 19.64%, 38.29%, and 37.54%, respectively, compared to the untreated control. Analysis revealed IC_{50} values of 101.67, 75.99, 102.83, and 99.54 μg/mL. These results suggest that these concentrations inhibit cell viability by 50%, with compound 3f causing the most significant reduction (19.64% of cells survive). Therefore, it exhibits the most potent cytotoxic effect at this concentration. Compared to Doxorubicin, which has a reported IC_{50} of 1.24 μg/mL under similar conditions, our compounds exhibit a lower but still notable cytotoxicity. The overall results of cytotoxicity tests for anticancer effects are greatly impacted by the kind, location, and number of substituents on aromatic rings. (Rao et al., 2025).

To further contextualize the anticancer activity of the synthesised compounds, a comparison with structurally linked pyrazoline and chalcone derivatives reported in the literature was conducted (Table 2). Previously reported pyrazoline derivatives evaluated versus the MCF-7 cell line generally exhibit IC_{50} values that depend on the substitution pattern and molecular framework. By comparison, the trisubstituted pyrazoline derivatives reported in the present study exhibit comparable or improved cytotoxicity, particularly for those bearing electron-donating and electron-withdrawing substituents. These results suggest that trisubstitution and rational electronic modulation enhance anticancer efficacy, thereby highlighting the advantages of the current molecular design. The absence of cytotoxicity evaluation in normal (non-cancerous) cells is now explicitly stated and highlighted as an important area for future investigation.

Figure 4. ^{19}FNMR Spectra of the Synthesized Compounds (2a, 2d) and (3e, 3f and 3h)

3.2.1 Molecular Docking Studies

Compounds 2a and 3f were shown to have strong anticancer effects on the MCF-7 cell line in laboratory tests, which supported their use in experiments. Molecular docking is an important part of the process of finding new drugs. In this study, MOE (Molecular Operating Environment) software was utilized to do molecular docking calculations and make predictions about how the prepared chemicals (2a and 3f) would bind to the protein (5T92) (Hussein et al., 2023) (Figure 7). There are expected binding affinities and features of compound (2a and 3f) toward (5T92) in Table 3. There are also the best positions for compound (2a and 3f) to bind to the target protein. There was a strong binding affinity between the substance that was studied and the fundamental amino acid residues of the

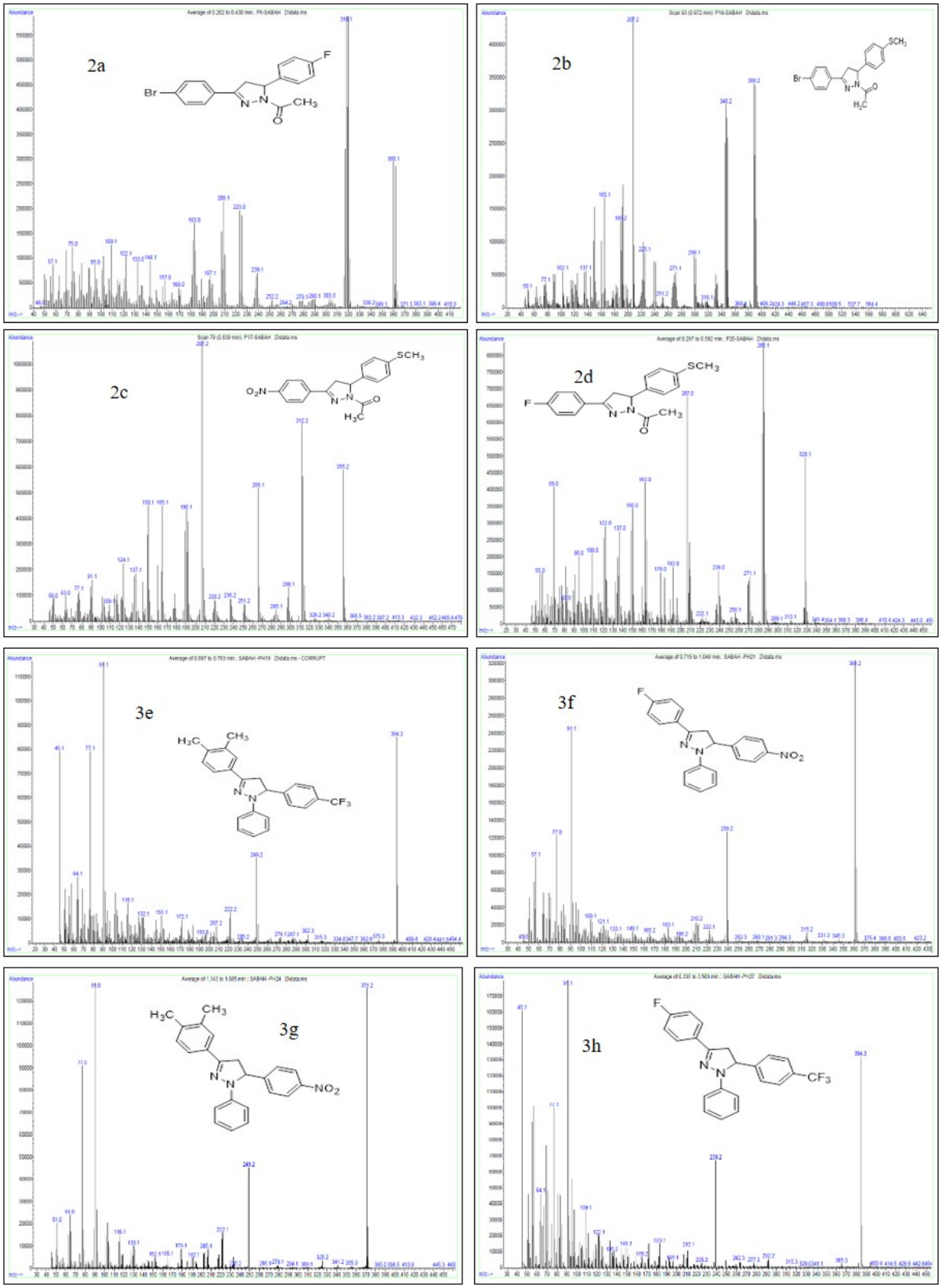

Figure 5. Mass Spectra of the Synthesized Compounds (2a-2d) and (3e-3h)

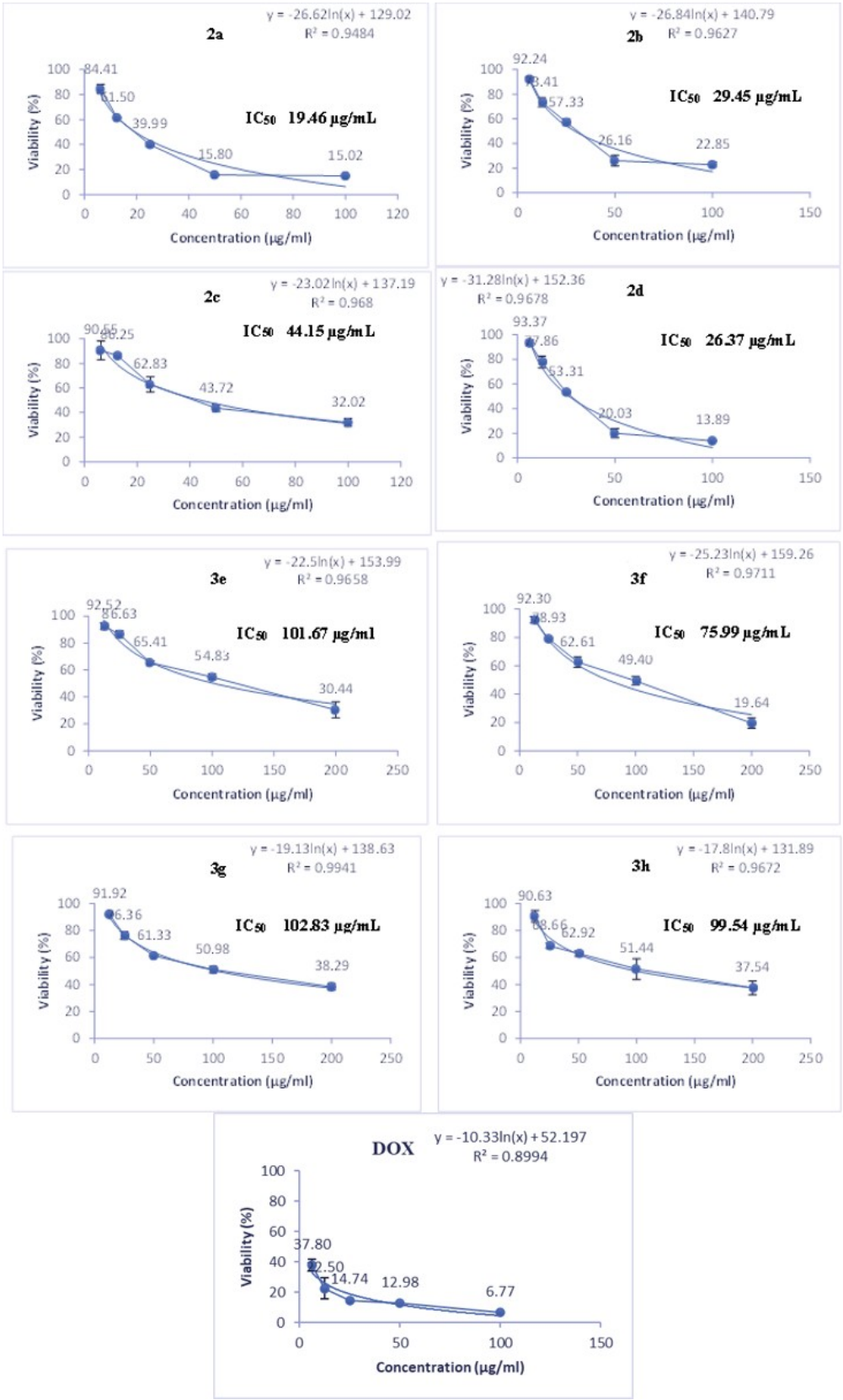

Figure 6. Cytotoxicity of the Synthesized Compounds (2a-2d), (3e-3h) and Doxorubicin Against the MCF-7 cell Line

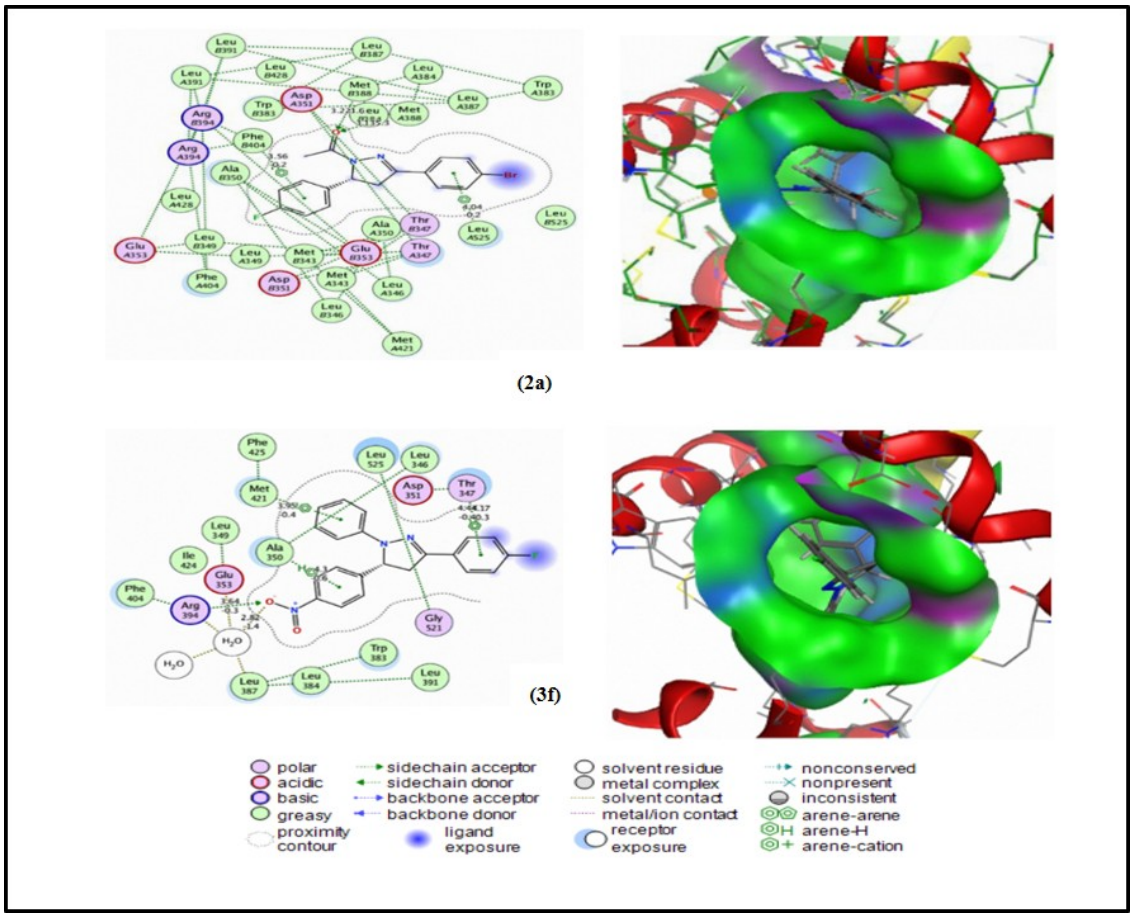

Figure 7. 2D and 3D of the Best Proses for Pyrazoline Derivatives 2a and 3f

Table 3. Details of the Best Poses of Ligands 2a and 3f with Protein 5T92

Comp. No.	Binding Affinity (Kcal/mol)	RMSD (Å)	Atom of Compound	Atom of Receptor	Involved Receptor Residues	Type of Interaction Bond	Distance (Å)	E (Kcal/-mol)
2a	-6.48797	1.621155	O20	CG	MET 388	H-acceptor	3.13	5.3
			O20	CG	MET 388	H-acceptor	3.22	1.6
			6-ring	CD2	LEU 525	pi-H	4.04	-0.2
			6-ring	CD1	PHE 404	pi-H	3.56	-0.2
					ARG 394	H-acceptor	3.64	-0.3
3f	-7.68887	1.301876	O27	NH2	HOH 705	H-acceptor	2.82	-1.4
			O27	O	THR 347	pi-H	4.44	-0.4
			6-ring	CA	THR 347	pi-H	4.17	-0.3
			6-ring	CG2	THR 347	pi-H	4.30	-0.6
			6-ring	CB	ALA 350	pi-H	3.95	-0.4

5T92 protein, which could be seen in both 2D and 3D models (PDB ID: 5T92). There are two main types of interactions, which have been shown by the interactions: hydrogen bonds and hydrophobic interactions. The interactions were looked

Table 4. Calculated ADME Properties of Compounds 2a and 3f In Silico

Comp.	Physicochemical Parameters							Absorption Distribution				
	M.wt ≤500	RB ≤5	HBA ≤10	HBD ≤5	MR 40–130	TPSA (Å^2) ≤140	Log $P_{o/w}$ −0.4 to +5.6	Water Solubility	Lipinski's Violation	GI	BBB	P-gp
2a	361.21	3	3	0	94.69	32.67	3.79	Poorly	0	High	Yes	No
3f	361.37	4	4	0	111.04	61.42	3.94	Poorly	MLOGP > 4.15	High	Yes	No

into more by measuring the hydrogen bonds and bond lengths inside the active site. That is, we looked at the root mean square deviation (RMSD) of the ligand's coordinates compared to the best estimated pose. Finding the best minimum-RMSD alignment is part of figuring out the RMSD numbers for each conformer. The root mean square deviation (RMSD) of the best pose for high-accuracy docking is usually between 1.301876 and 1.621155 Å. The pictures show that chemicals (2a and 3f) interact with different amino-acid components through proton donor, acceptor and hydrogen pi interactions. They also interact with water and other amino acids through two H-acceptor-pi-H interactions. The energy binding and distance of the contact are shown in Table 3. In general, these findings will help scientists make strong medicines that can be utilized to treat human breast cancer cell lines (MCF-7) (Al-Mutairi et al., 2024).

3.3 ADMET Analysis

We selected compounds 2a and 3f because they are sufficiently active to enable investigation of pharmacokinetic properties and ADMET (Absorption, Distribution, Metabolism, and Elimination) analyses. The Swiss ADMET web tool Bioinformatics (2024) is utilized for in silico ADMET (Absorption, Distribution, Metabolism, and Elimination) analysis to determine whether the designed compound exhibits a favourable pharmacokinetic profile or causes toxicity upon systemic administration. Every characteristic, including the number of rotatable bonds, molecular weight, topological polar surface area, molar refractivity of hydrogen-bond acceptors, consensus of computed lipophilicity, and number of hydrogen-bond donors, is comparable, as shown in Table 4. In addition to water, the solubility is moderate. In contrast, Table 4 shows that none of them violated Lipinski's rule, except compound 3f, which has one MLOGP (Moriguchi Octanol-Water Partition Coefficient) >4.15. Additionally, the compound's gastrointestinal (GI) absorption in humans is high, and it has robust blood-brain barrier (BBB) permeability, suggesting effective oral absorption. However, compounds do not interact with p-glycoprotein (P-GP) substrates, which could affect their oral absorption. Predicted outcomes indicate that the chemicals have favourable pharmacokinetic characteristics and could be turned into oral medications (Silva et al., 2021). Despite limitations, such as violations and deviations in values, they encourage the development of predictive models and the understanding of reactivity.

3.4 DFT Study

3.4.1 FMOs and Energy Gap

Softness, electron affinity, ionization potential, hardness, and chemical hardness are just a few of the molecular electronic properties that are always significantly influenced by frontier molecular orbitals (FMOs), such as the lowest unoccupied molecular orbital (LUMO) and the highest occupied molecular orbital (HOMO) (Abduljleel et al., 2023). Quantum-chemical indicators such as energy of the lowest unoccupied molecular orbital (ELUMO), energy of the highest occupied molecular orbital (EHOMO), energy gap (ΔE), softness, hardness, and dipole moment are calculated and shown in Table 5. An electron donor is the term used to describe the highest occupied molecular orbital (HOMO). While the lowest unoccupied molecular orbital (LUMO) is referred to as an electron acceptor due to its lack of electrons, it has more electrons. The three-dimensional shapes of the 2 orbitals are shown in Figure 8. One important determinant of the stability and reactivity of the compounds is the energy differential (ΔE) between the HOMO and LUMO energies. Molecules with great kinetic stability and low chemical reactivity are indicated by a significant energy gap (Rad et al., 2016; Al Shuhaib et al., 2023). Therefore, it is generally not favourable to move electrons from the lower HOMO orbitals to the higher LUMO (Hussein et al., 2023). The trends in the energy gap (ΔE) indicate that 2d >2a >2b >3e>3h>2c>3f>3g. These results suggest that 3g has the lowest kinetic stability and the highest chemical reactivity. Figure 8 illustrates the energy gap and the density of states. Based on the density of states (DOS) plot, the number of permitted electrons per energy period at every level of energy that can be filled is shown, and it also gives a general picture of the properties of the molecular orbitals in the energy gap of the molecule, which results from the simultaneous action of the donor and acceptor groups as well as the spacer's influence on electron delocalization (R. et al., 2023).

3.5 Hardness and Softness

One important chemical term in the conceptual DFT (Density Functional Theory) is chemical hardness (η). The ability of the electron cloud of atoms, ions, and molecules to withstand polarization is referred to as chemical hardness (Eşme et al., 2019). The estimated value for the chemical hardness (η) is ΔE/2 (H. et al., 2022). The trends of chemical hardness exhibit that 2d>2a >2b>3e>3h>2c>3f>3g (Table 5). Softness is the contrary

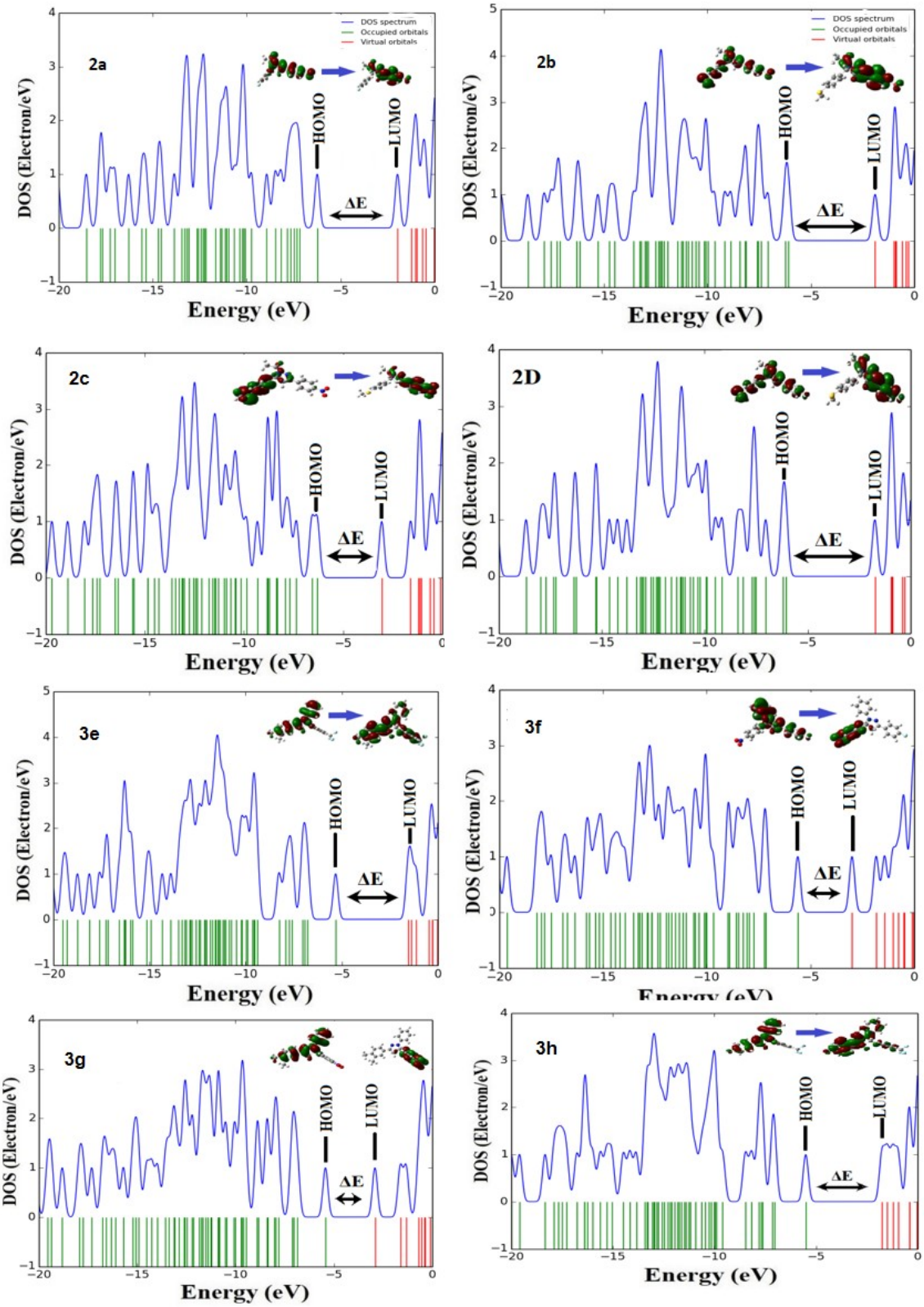

Figure 8. The FMOs and DOS Plot for Pyrazoline Derivatives 2a-2d, and 3e-3h at the B3LYP Level with the 6-311G+ (d) Basis Set

Table 5. Determined Values for the Quantum Chemical Indicators by B3LYP/6-311G+(d)

Chemical Quantum Descriptors	2a	2b	2c	2d	3e	3f	3g	3h
LUMO (eV)	-1.9709	-1.8857	-3.0479	-1.7281	-1.5534	-2.9897	-2.9072	-1.7510
HOMO (eV)	-6.2452	-6.0841	-6.2972	-6.0596	-5.3157	-5.6068	-5.4237	-5.4999
Egap (eV)	4.2743	4.1984	3.2493	4.3314	3.7622	2.6171	2.5165	3.7489
Hardness η (eV)	2.137	2.0992	1.6246	2.1657	1.8811	1.3085	1.2582	1.8744
Softness S (eV^{-1})	0.4679	0.4763	0.6155	0.4617	0.5315	0.7642	0.7947	0.5334
Dipole Moment μ (Debye)	5.409	5.106	10.140	5.030	4.302	4.158	5.867	2.627

Table 6. Calculated Nonlinear Optics of Compounds

Chemical Quantum Descriptors	2a	2b	2c	2d	3e	3f	3g	3h	Urea	PNA	2M4N
Polarisability (α)	252. 31	292. 21	297. 31	263. 39	327. 38	303. 43	334. 61	296. 32	33. 39	101. 3	113. 95
Hyperpolarizability (β)	372. 48	1098. 78	7560. 93	910. 16	2289. 61	1457. 35	1665. 35	1457. 35	71. 53	1670. 27	1671. 9

of hardness, S = $1/\eta$ (Bouzidi, 2018). The sequence of softness is 3g >3f >2c >3h >3e >2b >2a >3d (Table 5). The softness and hardness terms correspond to the energy gap of molecules. Molecules with smaller energy gaps will be softer and less complicated. Therefore, softer molecules are more conductive (R. et al., 2022), polarizable (Sajid et al., 2018), less kinetically stable (Li et al., 2022), and more chemically reactive (Khan et al., 2018). The dipole moment (μ) of a molecule is essential for a variety of chemical activities. Single dipole moments are produced when two atoms forming a chemical bond have distinct electronegativity (Aly, 2022; Manwar et al., 2025). The order of dipole moment (μ) shows that 2c>3g>2a>2b>2d>3e>3f>3h, as shown in Table 5. The quantum-mechanical characteristics of trisubstituted pyrazoline derivatives were statistically examined to determine whether the energy of the highest occupied molecular orbital (EHOMO), the lowest unoccupied molecular orbital (ELUMO), the energy gap (ΔE), softness, hardness, and dipole moment could serve as predictive indicators for anticancer. Based on Equation 1, there is a strong linear correlation between half-maximal inhibitory concentration (IC_{50}) and energy of highest occupied molecular orbital EHOMO. This suggests that the (EHOMO) determines the drug's binding affinity to the biological receptor.

$$IC_{50} = 566.66298 + 86.6893\, E_{\mathrm{HOMO}} \quad (1)$$

Correlation Coefficient (R) = 0.94052, and Standard deviation (SD) = 13.37655

However, the results of Equation (2) indicate that the energy of the lowest unoccupied molecular orbital (E_{LUMO}) exhibits a very weak linear correlation with the IC_{50} values. Equation (3) further demonstrates a moderate linear relationship between the observed IC_{50} values and the energy gap. Based on Equations (4) and (5), IC_{50} shows a moderate linear correlation with molecular softness and hardness, respectively. Finally, Equation (6) reveals a weak correlation between the dipole moment and the IC_{50} values.

$$IC_{50} = 47.48629 - 6.70463\, E_{\mathrm{LUMO}} \quad (2)$$

R= -0.11694 SD = 39.10318

$$IC_{50} = 174.11613 - 31.13339\, \Delta E \quad (3)$$

R= -0.6174 SD = 30.97296

$$IC_{50} = -29.02673 + 157.51181\, S \quad (4)$$

R= 0.57306 SD = 32.26688

$$IC_{50} = 174.10694 - 62.26317\, \eta \quad (5)$$

R= -0.61737 SD = 30.97398

$$IC_{50} = 95.71043 - 6.24366\, \mu \quad (6)$$

R= -0.37362 SD = 36.52194.

3.5.1 Properties of Nonlinear Optics

The compounds were also subjected to calculations and interpretations of the first hyperpolarizability (β), isotropic average polarisability (α), and dipole moment (μ), to investigate the connection between molecular structure and nonlinear optics (NLO) using hybrid functional (B3LYP) and the basis set 6-31G +(d) theory. The nonlinear optical properties of the compounds are listed in Table 6. Urea, para-nitroaniline (PNA), and 2-methyl-4-nitroaniline (2M4NA) were selected as references in this study because no experimental data were available on the nonlinear optics (NLO) characteristics of the materials under study. According to Table 6, compound 2c

has a higher isotropic average polarisability (α) and first hyperpolarizability (β) than the reference materials. This finding supports the use of these substances as materials for electro-optic and birefringent applications (Salman et al., 2022; Faisal et al., 2024).

4. CONCLUSIONS

In this research, eight trisubstituted pyrazolines were synthesized via cyclocondensation and characterised by NMR and EI-MS. They were then tested for cytotoxic activity against the breast cancer cell line MCF-7 and analysed using DFT (Density Functional Theory) methods. The results revealed that only compounds 2a and 3f exhibited significant anti-tumour activity, with half-maximal inhibitory concentrations (IC_{50}) of 19.46 μg/mL and 75.99 μg/mL against MCF-7, respectively. Molecular docking predicted the binding modes of compounds 2a and 3f with protein 5T92, revealing their best binding poses. The docking studies revealed favourable binding interactions that support the observed cytotoxicity, while DFT (Density Functional Theory) calculations provided insight into the electronic properties and stability of the synthesised compounds. Together, these findings demonstrate the value of integrating experimental and computational approaches to guide rational molecular design. However, the study is limited by evaluation against a single cancer cell line and the absence of selectivity and in vivo studies. Future work should focus on broader biological screening, mechanistic investigations, and further structural optimisation to improve anticancer strength and discrimination. The absence of cytotoxicity evaluation in normal cells is now explicitly acknowledged as a limitation and a focus for future studies.

5. ACKNOWLEDGMENT

The authors sincerely acknowledge the University of Basrah in Iraq for its assistance in achieving the ^{1}H and ^{13}C NMR spectra required to complete the study.

REFERENCES

Abbas, K. H., N. A. Salman, and A. S. Alwan (2024). Synthesis, Anticancer Activity, and Computational Studies of New Pyrazole Derivatives. *Russian Journal of General Chemistry*, **94**(3); 719–728

Abduljleel, A. M., J. M. S. Alshawi, K. A. Hussein, and S. M.-H. Ismael (2023). Synthesis, Characterization, Biological Studies and DFT Study of Schiff Bases and Their Complexes Derived from Aromatic Diamine Compounds with Cobalt (II). *Revista Bionatura*, **8**(1); 61

Abou-Zied, H. A., E. A. M. Beshr, A. A. M. Hayallah, and I. M. Abdel-Rahman (2024). Emerging Insights into Pyrazoline Motifs: A Comprehensive Exploration of Biological Mechanisms and Prospects for Future Advancements. *Journal of Molecular Structure*, **1296**; 136807

Al-Mutairi, L. A., S. H. Al-Shehri, and A. M. Al-Harbi (2024). New Pyrazole/Pyrimidine-Based Scaffolds as Inhibitors of Heat Shock Protein 90 Endowed with Apoptotic Anti-Breast Cancer Activity. *Pharmaceuticals (Basel)*, **17**; 1284

Al Shuhaib, Z., K. A. Hussein, and S. M. Ismael (2023). Synthesis of New Pyrimidine Derivatives, Study of Anti-Cancer Activity, Structural Properties, and Molecular Docking. *Russian Journal of General Chemistry*, **93**; 1171–1180

Ali, K. H., A. M. Alwan, and Z. H. Jasim (2020). Design, Synthesis, Characterization, and Cytotoxicity Activity Evaluation of Mono-Chalcones and New Pyrazolines Derivatives. *Journal of Applied Pharmaceutical Science*, **10**(08); 020–036

Ali, N. H., M. S. Hassan, and L. A. Al-Mutairi (2024). Synthesis, In Silico ADMET Prediction Analysis, and Pharmacological Evaluation of Sulfonamide Derivatives Tethered with Pyrazole or Pyridine as Anti-Diabetic and Anti-Alzheimer's Agents. *Saudi Pharmaceutical Journal*, **32**(5); 102025

Alsimaree, A. A. (2025). Recent Advances on Antiproliferative and Anti-Inflammatory Potential of Pyrazoline Derivatives. *Biointerface Research in Applied Chemistry*, **15**; 1–19

Aly (2022). Structural, Spectroscopic, FMOs, and Non-Linear Optical Properties Exploration of Three Thiacalix[4]Arenes Derivatives. *Arabian Journal of Chemistry*, **15**(3); 103656

Baskerville, A. L., M. Targema, and H. Cox (2022). Reparametrization of the Colle–Salvetti Formula. *Royal Society Open Science*, **9**(1); 211333

Becer, E., E. M. Altundağ, M. Güran, H. S. Vatansever, S. Ustürk, D. Y. Hanoğlu, and K. H. C. Başer (2023). Composition and Antibacterial, Anti-Inflammatory, Antioxidant, and Anticancer Activities of Rosmarinus officinalis L. Essential Oil. *South African Journal of Botany*, **160**; 437–445

Bioinformatics, S. I. (2024). SwissADME. http://www.swissadme.ch/

Bouzidi, M. (2018). Inhibitive Properties and Quantum Chemical Calculations of a New Synthesized Schiff Base 1-[(3-Hydroxyphenylamino)Methylene]-Naphthalen-2-One for XC48 in Hydrochloric Acid Solution. *International Journal of Electrochemical Science*, **13**(7); 6734–6755

Chemical Computing Group ULC (2025). Molecular Operating Environment (MOE)

Dadang, D. (2025). Discovery of Pyrazoline Benzenesulfonamide Derivatives as Anticancer Agents: A Review. *Drug Design, Development and Therapy*, **19**; 11697–11747

Dimitris, D. (2020). Pyrazoline Hybrids as Promising Anticancer Agents: An Up-to-Date Overview. *International Journal of Molecular Sciences*, **21**(15); 5507

El-Sayed, N. A., R. M. Ibrahim, and E. S. Mahmoud (2022). Synthesis of Chalcones Derivatives and Their Biological Activities: A Review. *ACS Omega*, **7**; 27769–27786

Elkanzi, N. A. A., H. Hrichi, R. A. Alolayan, W. Derafa, and F. M. Zahou (2022). Synthesis of Chalcones Derivatives and Their Biological Activities: A Review. *ACS Omega*, **7**(32); 27769–27786

Eşme, A., S. Sağlam, and F. Kandemirli (2019). Theoretical Investigation on the Molecular Structure, Electronic, Spectroscopic Studies and Nonlinear Optical Properties of 5-Bromo-1-(2-Cyano-Pyridin-4-yl)-1H-Indazole-3-

Carboxylic Acid Diethylamide: A DFT and TD-DFT Study. *Acta Physica Polonica A*, **136**(3); 378–394

Faisal, A. G., Q. M. A. Hassan, T. A. Alsalim, H. A. Sultan, F. S. Kamounah, C. A. Emshary, and K. A. Hussein (2024). Curcumin Analogue: Synthesis, DFT and Nonlinear Optical Studies. *Optik*, **306**; 171800

Frisch, M. J. (2016). Gaussian. Gaussian Inc.

H., S., D. M., and Y. O. (2022). Atoms-in-Molecules' Faces of Chemical Hardness by Conceptual Density Functional Theory. *Molecules*, **27**(24); 8825

Hameed, W. A., I. A. Hameed, and N. A. Ali (2025). Synthesis, Identification, and Biological Evaluation of New Coumarin-Pyrazoline Derivatives as Anti-Oxidant Agents. *Baghdad Science Journal*, **22**(1); 16–35

Hassan, Z. A., L. A. Al-Mutairi, and N. H. Ali (2024). Exploring 2-Pyrazoline Derivatives as Potent Antidiabetic Agents and Cholinesterase Inhibitors: Their Synthesis and Molecular Docking Studies. *Journal of Molecular Structure*, **1315**; 138978

Hussein, K. A., Z. Al-Shuhaib, and S. M. H. Ismael (2023). Synthesis, Biological Activity, and Computational Examination of New 3-Cyano-2-Oxapyridine. *Tropical Journal of Natural Product Research*, **7**(11); 5270–5278

Khan, M. A., F. N. Ahmed, and S. M. Ali (2018). Molecular Modeling, pKa and Thermodynamic Values of Asthma Drugs. *Medicinal Chemistry Research*, **27**; 95–114

Khan, R. A., S. M. Ali, and F. N. Ahmed (2026). Redox-Responsive and Electronically Adaptive Ferrocenyl-Pyrazoline: Bond Softening, Rydberg Interactions, and Antibacterial Mechanism. *Journal of Molecular Structure*, **1354**; 144901

Khan, Y. A., R. A. Ali, and S. M. Ahmed (2024). In Silico Evaluation of Novel 2-Pyrazoline Carboxamide Derivatives as Potential Protease Inhibitors Against Plasmodium Parasites. *Chemistry Proceedings*, **16**(1); 57

Li, Q., W. Zhang, and J. Chen (2022). Excellent Magnetic Softness-Magnetization Synergy and Suppressed Defect Activation in Soft Magnetic Amorphous Alloys by Magnetic Field Annealing. *Journal of Materials Science & Technology*, **116**; 72–82

Manwar, H. Q., Z. Al-Shuhaib, K. A. Hussein, and S. M. H. Ismael (2025). Synthesis, Computational and Anti-Cancer Activity Studies of New 5-Substituted Tetrazole-1-yl Acetamides. *Chemistry Africa*, **8**; 1271–1286

Nair, M. R., P. S. Menon, and A. K. Thomas (2022). Carbon Dots: A Study of Its Cytotoxic Activity Against HepG2 and MCF-7 Cell Lines. *Materials Today: Proceedings*, **49**; 608–612

Nair, R. S., A. K. Thomas, and P. S. Menon (2025). Exploring Pyrazolines as Potential Inhibitors of NSP3-Macrodomain of SARS-CoV-2. *Scientific Reports*, **15**; 767

Nehra, B., M. Kumar, V. Chawla, and P. A. Chawla (2025). Current Progress in Synthetic and Medicinal Chemistry of Pyrazole Hybrids as Potent Anticancer Agents with SAR Studies. *Future Journal of Pharmaceutical Sciences*, **11**; 75

Patil, V. R., A. P. Kumar, and K. S. Reddy (2024). Synthesis, Molecular Docking, and Biological Evaluation of Some New Naphthalene-Chalcone Derivatives as Potential Anticancer Agent on MCF-7 Cell Line by MTT Assay. *Asian Journal of Green Chemistry*, **8**; 234–246

R., P., R. V., and R. N. (2022). Density Functional Theory, Chemical Reactivity, and the Fukui Functions. *Foundations of Chemistry*, **24**; 59–71

R., S., K. P., and S. V. (2023). A DFT Study of Vibrational Spectra of 5-Chlorouracil with Molecular Structure, HOMO–LUMO, MEPs/ESPs and Thermodynamic Properties. *Polymer Bulletin*, **80**; 3055–3083

Rad, A. S., M. Esfahanian, E. Ganjian, and H. allah Tayebi (2016). Ab-Initio Study of Physisorption of Hydrogen Cyanide on 2PANI: A Model for Polyaniline Gas Sensor. *Zeitschrift für Physikalische Chemie*, **230**(10); 1487–1498

Rao, P. R., K. S. Reddy, and A. P. Kumar (2025). Synthesis of Fluoro and Nitro Pyrazoline Derivatives: Anticancer and Molecular Docking Studies. *Multidisciplinary Journal Centering on Chemistry*, **90**; e202500024

Reddy, P. K., S. Babu, and D. M. Rao (2025). Substitution Induced Solvatochromism Behaviour of Blue Emissive N-Aryl Pyrazoline Derivatives and DFT Studies. *Journal of Luminescence*, **281**; 121200

Reddy, S. K., K. S. Rao, and P. M. (2024). Pyrazole Derivatives: A Comprehensive Review of Their Multifaceted Biological Activities and Therapeutic Potentials. *International Research Journal*, **11**; a659–a666

Sajid, H., M. Zubair, M. Imran, M. Bilal, and M. Shahid (2018). High Sensitivity of Polypyrrole Sensor for Uric Acid Over Urea, Acetamide and Sulfonamide: A Density Functional Theory Study. *Sensors and Actuators B: Chemical*, **235**; 49–60

Salman, U. A., N. A. Ali, and H. A. Mohammed (2022). Optical Nonlinear Properties and All Optical Switching in a Synthesized Liquid Crystal. *Journal of Molecular Liquids*, **361**; 119676

Silva, L. M., C. R. Oliveira, and M. P. Santos (2021). Structural Optimization and Biological Activity of Pyrazole Derivatives: Virtual Computational Analysis, Recovery Assay and 3D-Culture Model as Potential Predictive Tools of Effectiveness Against Trypanosoma Cruzi. *Molecules*, **26**(21); 6742

Yadav, C. S., I. Azad, A. R. Khan, M. Nasibullah, N. Ahmad, D. Hansda, S. N. Ali, K. Shrivastav, M. Akil, and M. B. Lohani (2024). Recent Advances in the Synthesis of Pyrazoline Derivatives from Chalcones as Potent Pharmacological Agents: A Comprehensive Review. *Results in Chemistry*, **7**; 101326

Zhang, L. Y., W. Chen, and F. Li (2020). Synthesis and Biological Evaluation of Amino Chalcone Derivatives as Antiproliferative Agents. *Molecules*, **25**(23); 5530

